Dynamics and style transition of a moderate, Vulcanian-driven eruption at Tungurahua (Ecuador) on February 2014: pyroclastic deposits and hazard considerations

Jorge Eduardo Romero[1], Guilhem Amin Douillet[2], Silvia Vallejo Vargas[3], Jorge Bustillos[4], Liliana Troncoso[4], Juan Díaz Alvarado[1], and Patricio Ramón[3]

[1]Departamento de Geología, Universidad de Atacama, Copiapó, Chile
[2]Earth and Environmental Sciences, Ludwig-Maximilians-Universit'at, Munich, Germany
[3]Instituto Geofísico, Escuela Politécnica Nacional, Quito, Ecuador
[4]Escuela de Geología, Facultad de Geología, Minas, Petróleos y Ambiental (FIGEMPA), Universidad Central del Ecuador Quito, Ecuador

Correspondence to: Guilhem Amin Douillet (g.douillet@min.uni-muenchen.de)

Abstract. The ongoing eruptive cycle of Tungurahua volcano (Ecuador) since 1999 has been characterized by over 15 paroxysmal phases interrupted by periods of relative calm. Those phases included Strombolians, Vulcanians and one Subplinian eruptions and they generated tephra fallouts, pyroclastic density currents (PDCs) and lava flows. The 01 February 2014 eruption occurred after 75 days of quiescence. Two days before the eruption, a gradual increase of seismicity associated with sporadic

5   weak ash emissions occured. Between 13:30 and 16:30 UTC of the 01 February, a swarm of volcano tectonic and long period earthquakes was detected and announced the possibility of an eruption within hours or days. After a few hours without surface manifestations, two short-lived Vulcanian explosions triggered the paroxysmal phase at 22:39 UTC which lasted 40 min and produced an eruptive column 13.4 km in height sustained during about 9 min. The activity evolved at 23:36 UTC into sporadic Strombolian explosions with discrete ash emissions and continued for several weeks.

10   Both tephra fall and PDCs were studied for their dispersal, sedimentology, volume and eruption source parameters. Tephra was distributed around $240°$ to the S-SW of the volcano, and the bulk deposit volume is estimated to be $1.53 \pm 0.35 \ 10^{-2} \ km^3$ $(4.76 \pm 2.23 \ 10^6 \ m^3$ DRE; VEI 3). PDCs descended by 9 ravines of the N-NW flanks. It was one of Tungurahua's largest eruptions, after the August 2006 Subplinian event. The Vulcanian eruptive mechanism is interpreted to be related to a steady magma ascent and the rise in over-pressure in a blocked conduit (plug) and/or a depressurized solidification front. The transition

15   to Strombolian style is well documented from the tephra fall componentry. In any of the interpretative scenari, the short-lived precursors for such a major event as well as the unusual tephra dispersion pattern urge for renewed hazard considerations at Tungurahua.

1 Introduction

In comparison to Strombolian or Plinian fallout deposits, Vulcanian fine grained fallout deposits often lack a sufficient preser-

20   vation potential for extensive studies from proximal to distal portions (Rose et al., 2008). Generally, these eruptions produce

predominantly fine-ash to lapilli sized tephra which is dispersed to heights < 20 km, and last on the order of minutes (Morrissey and Mastin, 2000). Vulcanian events commonly originate from andesitic or dacitic magma composition (*e.g.*, Cas and Wright, 1987; Cole et al., 2015; Hall et al., 2015; Zobin et al., 2016). Typically, the juvenile ejected material is dominated by block to fine-ash size tephra with poor to moderate vesicularity, angular shape and vitric to crystalline texture (Morrissey

5 and Mastin 2000). Non-juvenile rocks make a major fraction of the ejected material. All those observation are interpreted to show the progressive deepening of the source in the magma conduit, brittle fragmentation of highly viscous magma and high explosivity (*e.g.*, Clarke et al., 2015). The ejected tephra thus help to constrain the source depth and intensity of the eruption. Vulcanian eruptions can be associated with the generation of pyroclastic density currents (PDCs, *e.g.*, Brown and Andrews, 2015), especially if they trigger moderate andesitic eruptions, which are more prone to produce PDCs than other eruption types

10 (Bernard et al., 2016). Although the transitional behaviors of Vulcanian eruptions from/to Subplinian and Strombolian eruptions are occasionally observed (Maeno et al., 2013), these changes in the eruptive style are not widely described and claim attention, in particular for volcanic hazard assessment.

This study focuses on the pyroclastic deposits associated with the eruptions from 1-14 February 2014 of Tungurahua volcano (Ecuador). Tephra fallout and PDC erupted material are described and used to infer the style transition, eruption magnitude and

15 source parameters. Special attention is given to explain the unusual rapid evolution from unrest to eruption, and the possible existence of a plug in the conduit. The deposits and flow of PDCs are also described and discussed. The meaning of this eruption is put in perspective with the context of Tungurahua's ongoing cycle.
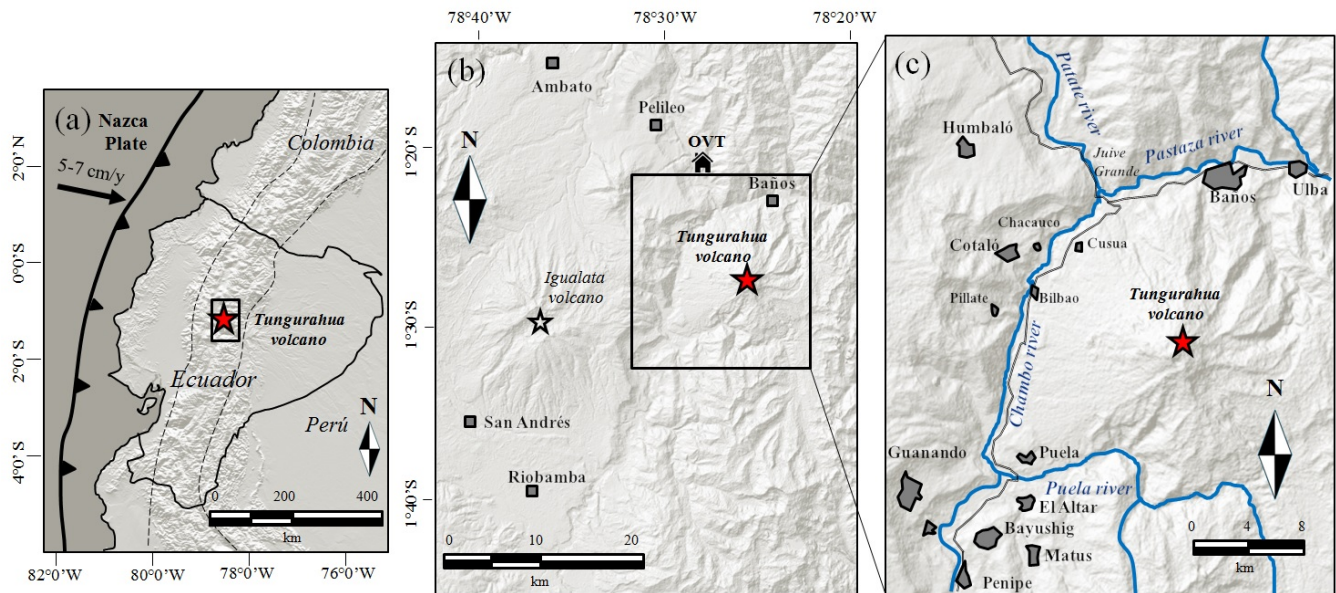

Figure 1. Location map of Tungurahua volcano. (a) Geodynamic context of the Ecuadorian Andes (Ecuadorian volcanic arc is between dashed lines), (b) the main cities around Tungurahua and the OVT office, (c) proximal area around Tungurahua with towns and rivers.

1.1 Historical activity of Tungurahua

Tungurahua stratovolcano ($01°28'S$, $78°27'W$, $5019\ m\ a.s.l.$, Fig. 1) is among the most active Ecuadorian volcanoes, with five post Columbian eruptions (1641-46, 1773-81, 1886-88, 1916-18 and 1999-to-present; Hall et al., 1999; Le Pennec et al., 2008; Hall et al., 2013). The ongoing eruptive cycle (1999-present) has consisted of short periods of low-to-moderate Strombolian

5   activity with lava fountaining, Vulcanian explosions, lava flows, and PDCs (Douillet et al., 2013b, a; Hall et al., 2013, 2015). Tephra fallout from these eruptions is constituted by mostly asymmetric isopachs distributed toward the west, controlled by the regional wind direction (Bustillos, 2010; Eychenne et al., 2012, 2013; Bernard et al., 2013; Bustillos et al., 2016).

The largest eruption of the cycle (up-to-present) occurred on 17 August 2006. It produced a plume that reached a height of 18 km (Eychenne et al., 2012) and PDCs which descended 17 valleys located around the summit (Kelfoun et al., 2009;

10   Douillet et al., 2013b, a), as well as Aa lava flows on the upper flanks. The eruption affected for many years the villages of Cusúa, Chacauco, Bilbao and Juive-Grande as well as national roads around the volcano (Samaniego et al., 2008; Kelfoun et al., 2009; Hall et al., 2013). Prior to the eruptions of July and August 2006, deep (10-15 km depth) long period (LP) seismicity and edifice inflation were registered from April to May 2006 (Champenois et al., 2014). PDCs have become more frequent since 2008, with occurrence in 2008, 2010, 2011, 2012 and 2013, affecting livestock and agriculture on the flanks of the volcano.

15   The character of eruptions has remarkably evolved from Strombolian to a Vulcanian-dominated activity since 2010 and the frequency of eruptions has increased from 2006 up to present, doubling the tephra discharge rate (Bustillos et al., 2016, and references therein). Volcano degassing evolved from a more-or-less continuous activity between 1999 and late 2008, to episodic activity without significant degassing during quiescence periods (Arellano et al., 2008; Hidalgo et al., 2015). In mid-2013 and continuing until mid-2014, a cycle of Vulcanian explosions often associated with PDCs began, possibly linked to the plugging

20   of the conduit (Hall et al., 2015). The eruption of 14 July 2013, occurred after two months of quiescence and weak degassing, producing a 8.8 km high eruption column accompanied by a series of PDCs descending in at least nine valleys of the flanks up to 7.5 km from the cone (Hall et al., 2015; Parra et al., 2016).

1.2 The February 2014 eruption

A precise description of the February 2014 eruption chronology is summarized hereafter from the reports of the Instituto

25   Geofísico of the Escuela Politécnica Nacional from Quito (IG-EPN). It is based on the robust monitoring network of the Observatory of Volcano Tungurahua (OVT; http://www.igepn.edu.ec). From 13 November 2013 to 29 January 2014, the volcano experienced 77 days without any eruptive activity apart for a weak background degassing. On 30 January 2014, a new eruptive phase begun with an increase in seismic activity and few sporadic explosions accompanied by tephra fallout distributed toward the SW (Instituto Geofísico, 2014a). After a reduction in seismicity on 31 January, the seismic activity increased again dramat-

30   ically on 01 February between 01:10 and 20:30 UTC (Ecuadorian local time + 5:00 h), with a swarm of volcano-tectonic (VT) and long period (LP) events. At 17:00 UTC, the OVT reported to the Decentralized Government of Baños Risk Management Department (SGR, GAD-Baños) and through a public announcement, concerning the evolving seismic activity and increased possibility of eruption. The first large explosion occurred at 22:12 UTC, and produced a 5 km high column accompanied by
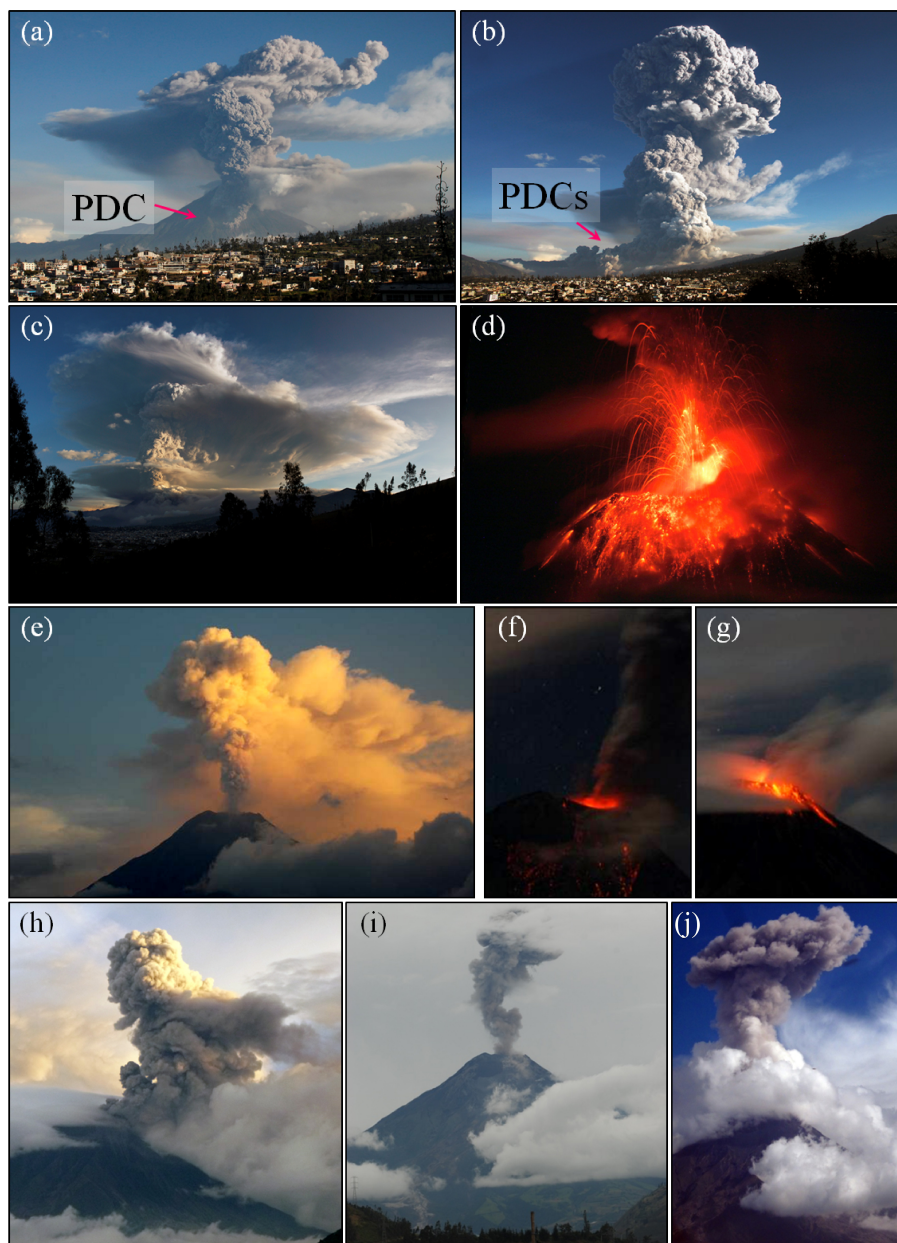
Figure 2. Evolution of the 01 February eruption. (a) Second Vulcanian explosion at 22:22 UTC on 01 February 2014 with the formation of PDCs flowing down the west flank of the volcano. (b) Rise in the explosive activity during the third Vulcanian explosion at 22:39 UTC with PDCs descending by the streams of the NW and W flanks of the volcano. (c) Development of multiple dispersion plumes at different fly levels of the eruptive column during the paroxysmal phase. (d) Strombolian activity as seen at 01:35 UTC on 02 February 2015 (Photos from (a) to (d) were taken by Raúl Díaz from city of Ambato). (e) Ash emissions on 07 February (Francisco Vázconez). (f) and (g) illustrate the Strombolian activity observed on 09 and 10 February 2015 (Francisco Vázconez and Pedro Espín). (h), (i) and (j) represent minor ash emissions observed on 10, 13 and 14 February 2015, respectively (Photos by Pedro Espín, Andrés Ordoñez and main author). The photos from (e) to (j) were taken from the OVT

PDCs that descended 0.5 km down the NW flank (Instituto Geofísico, 2014b). Another explosion at 22:32 UTC generated a new burst of PDCs with a similar distribution (Instituto Geofísico, 2014b, Fig. 2a). The third explosion at 22:39 UTC, was the trigger of the major Vulcanian eruption, and was associated with the largest PDCs (Instituto Geofísico, 2014c, Fig. 2b). These PDCs branched into at least 9 ravines from the N, W and SW flanks of the volcano down to the base of the edifice. Hall et al.

5 (2015) estimated the PDC flow velocities at 9.5-36 m/s. The paroxysm persisted for 42 min (Fig. 2c), but the highest sustained eruption column of 13.7 km lasted only 9 min (http://www.ssd.noaa.gov/VAAC/messages.html). A second eruptive phase dominated by fountaining Strombolian activity started at 23:36 UTC with ejection of incandescent bombs up to 0.8-1.0 km above the crater (Fig. 2d), shock waves (pressure waves?) and explosions felt up to 20-30 km from the crater (Instituto Geofísico, 2014d). The evacuation in Chacauco and Cusúa (W flank), as well as Bilbao and Juive-Grande (N-NW flank) took

10 place at 23:44 UTC. Tephra fallout up to lapilli grain size was reported in the localities of Pillate, Capil and Palictahua (6-7 km from the vent) and the eruption cloud resulted in total darkness at Chacauco village. A deflation of 340 μrad was observed subsequently to the end of the eruption, and following the inflation trend that was observed since October 2013 at RETU tilt meter (Vallejo et al., 2014). After this main episode, the activity continued with sporadic Strombolian explosions and discrete emissions of material decreasing in frequency over the whole February (Fig. 2e-j).

15 2 Sampling and analytical methods

2.1 Sampling and analysis of tephra deposits

The field surveys on the fallout deposit were carried out two weeks after eruption. We selected 23 locations with plane surfaces covered by tephra fallout without apparent reworking in order to measure deposit thickness and describe the sedimentological characteristics of the two weeks of eruption. Tephra samples were analyzed in terms of lithologic components. Four samples

20 were sieved manually in 0.5 ϕ intervals: B1 and C1 from 1 to 4 ϕ; C2 and SJ from -2.0 to 4.0 ϕ, with ϕ=-$log(2D/D_0)$ (D is the particle diameter and D_0 = 1 mm). The calculation of grain size parameters (*e.g.*, Otto, 1939; Inman, 1952; Folk and Ward, 1957; Cas and Wright, 1987; Murcia et al., 2013) was obtained with the Gradisat package (Blott and Pye, 2001).

Two isopach maps were hand-drawn for the proximal and distal areas of pyroclastic fall deposit. Bulk tephra volumes were calculated by the integration of 6 isopachs (two straight-line segments) using the models of exponential thinning (Pyle, 1989,

25 1995; Fierstein and Nathenson, 1992), Power Law (Bonadonna and Houghton, 2005) and Weibull (Bonadonna and Costa, 2012).

Bulk geochemistry was performed on a juvenile scoria sample using a Bruker X-Ray fluorescence (XRF) analyzer for semi-quantitative chemical analysis. Thin sections for petrographic description were obtained from a juvenile scoria of the Juive PDC deposits and were analyzed under a polarized light microscope.

30 We used the wind Reanalysis code (Palma, 2013) for reconstructing the statistical wind directions in the area of Tungurahua, using 32140 wind direction tendencies at 15 km a.s.l. from the 1999-2011 period, and another 7940 tendencies for the period January-March at the same altitude.

Solid Earth
Discussions

Geostationary Operational Environmental Satellite (GOES) 8 and 13 imagery, combined with the information of VAAC reports (http://www.ssd.noaa.gov/VAAC/ARCH14/TUNG/), were used to describe the tephra dispersion during the eruption.
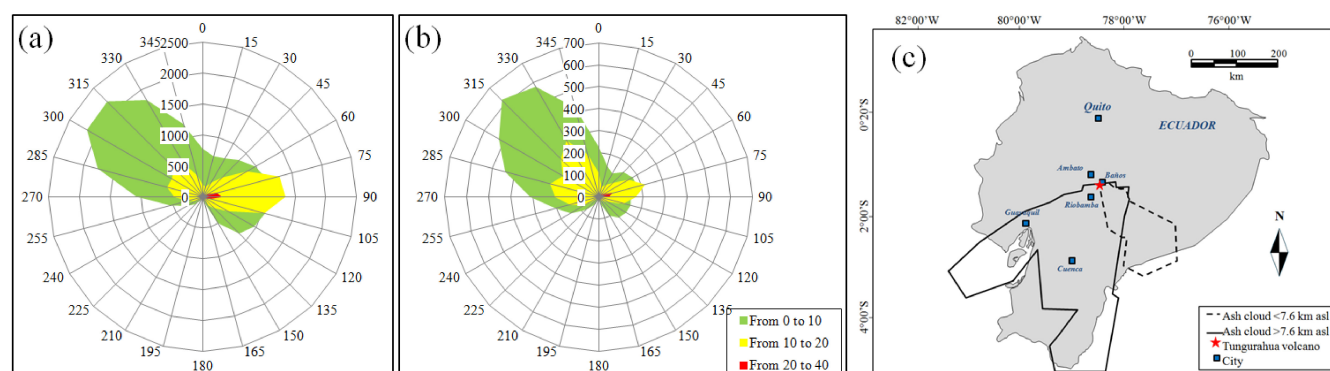

Figure 3. Wind patterns and plume dispersion. (a) and (b) Rose diagrams showing the frequency of the wind direction at an altitude of 15 km a.s.l. during the whole year and from January to March (data acquired from 1999 to 2011). The color of the series represent the wind speed measured in m/s. (c) Ash cloud dispersion during the 01 February 2015 eruption at different fly levels (<7.6 and >7.6 km a.s.l.), as obtained from VAAC.

2.2 Sampling and analysis of PDC deposits

The PDC deposits were observed in the field between the 08 and 25 February. Twenty-two samples from these deposits were sieved mechanically in $0.5\ \phi$ steps with a shaker from Retsch. The sieving protocol was 15 min shaking in intervals of 20 sec steps with a brief pause between each step for the whole fraction. The fraction $< 0.5\ mm$ was additionally shacked for 5 min in 10 sec intervals. This protocol was chosen to ensure the lowest amount of clast-abrasion during sieving. Further, the fine fraction ($< 125\ \mu m$) was analyzed with a laser-diffraction particle-size-analyzer (LS230 from Coulter). For this, each sample was measured five times with three consecutive runs, with the final result taken as the average of all runs.

3 Deposits of the 01 February 2014 eruption

3.1 Dynamics characteristics

Over the area of Tungurahua, annual wind directions at an altitude of 15 km a.s.l. mostly blow toward the NW with speed magnitudes of 0 to 20 m/s whereas the January to March tendency is NW for speeds of 0 to 10 m/s, but mostly E for speeds of 10 to 20 m/s (Fig. 3a, 3b). In all the time series, less than 1% correspond to S-SW directions (180 to 210° azimuth). The Washington Volcanic Ash Advisory Center (VAAC) reported a column height of 13.72 km after 22:45 UTC on 01 February 2014 (http://www.ssd.noaa.gov/VAAC/ARCH14/TUNG/2014B020235.html). The tephra cloud was mainly dispersed in a very uncommon pattern toward the SW and S-SW, being divided into two fly levels (<7.6 and >7.6 km a.s.l., Fig. 3c). The column

Table 1. Location of the most distal PDC front deposits.

Ravine	Vascún	Juive Pampa	Juive Grande	Juive v.-minero	Hacienda	Achupashal	Achu-west	Romero	Rea
North	0785961	0782360	0782307	0782442	0780052	0779307	0779944	0777198	0779504
East	9841782	9843861	9843030	9842270	9842785	9839171	9840256	9837637	9836248

Northing and Easting in m. Coordinate system: WGS84 - zone South West 17

source was associated with a hotspot on the Goes-13 McIDAS images with hottest pixel reaching 65° C. As measured from the images of the GOES-8 satellite, the plume was dispersed to 185° azimuth, with an average speed of 42.3 km/h, and an expansion of *ca.* 0.16 km^2/s with a total area of over 12 000 km^2 during the first 3.5 h after the eruption onset.

PDCs were mainly generated during the second (22:32) and third (main, 22:39) major explosions on 01 February. Direct and thermal footages (IG, www.igepn.edu.ec) reveal that the 2nd explosion was accompanied by PDCs flowing only in the upper flanks (ca. 500 m below crater). The third explosion developed at least two PDC pulses that flowed down the 9 ravines of the flanks (Table 1, Fig. 5). A first pulse in the upper Achupashal drainage surpassed the previous flows and flowed down to ca. 3500 m a.s.l. on the NW flank. The second pulse was greater, with PDCs flowing rapidly down the SW valleys (Rea and Romero) and apparently simultaneously filled the upper Achupashal and Juive drainages as well as the Vascún valley. It seems that PDCs were much faster in the Vascún valley than in the Achupashal drainage, and that the slowest descending flows were those from the Juive drainage.

3.2 Distribution and volume

The tephra fallout field study was carried out in mid-February, and thus contain the signature of two weeks of activity (between 01 and 14 February). Fallout distribution is well constrained on land at <20 km from the vent (Fig. 4a) but scarce data has been obtained in the distal areas (>20 km.) Whole tephra fall deposit mapped covers almost 13 000 km^2 with a nearly elliptic distribution dispersed toward the S-SW. This suggests that most of the distal deposit here studied correspond to the 01 February explosions. The thickest deposit (∼1 cm) was measured in a radius of about 9 km from the crater and following the dispersal axis whereas >1 mm deposit is distributed <30 km around the vent (Fig. 4a). Ash traces (∼0.1-1.0 mm thickness) were identified through the social media geo-referenced photography sent by people to the IG-EPN at distal areas on the main dispersion axis (*e.g.* Loja, 290 km S). The calculated volume of tephra fall deposit ranges from ∼0.97 to ∼2.37 10^{-2} km^3 , depending on the model (Table 2). Using a bulk deposit density supposed to be 760 kg/m^3, this leads to a total erupted mass between ∼0.74 to ∼1.80 10^{10} kg and total Dense Rock Equivalent (DRE) volume from ∼3.0 to ∼7.34 10^6 m^3 (Table 2). In consequence, our mean bulk tephra volume estimate is 1.53±0.35 10^{-2} km^3 (4.76±2.23 10^6 m^3 DRE).

PDCs branched into at least 9 valleys from the N, W and SW flanks of the volcano and reached the base of the edifice in several locations, endangering the main road of the area (Fig. 4b). According to Hall et al. (2015) the deposit lengths and
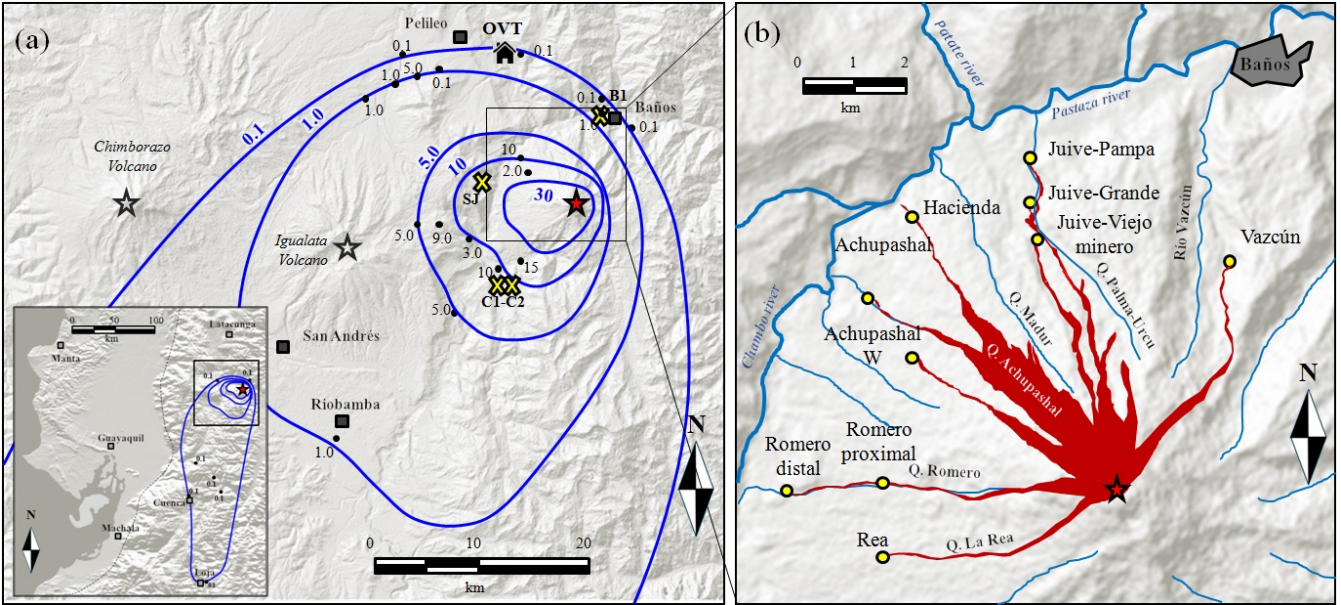
Figure 4. Pyroclastic deposits of the February 2014 eruption of Tungurahua volcano. (a) Isopach maps (blue lines, in mm) of tephra fall deposits associated to the 01-14 February 2014 eruptive period. Maps derived from 21 field measurements (black circles), yellow crosses are sampling sites for grain size analysis. See Fig. 5 for details on the field observations. (b) Distribution of PDCs from the 01 February eruption (red area), modified after Hall et al. (2015). Yellow circles represent the position for the field observation of PDC fronts (Table 1).

Table 2. Volume, mass and source parameters for the tephra fall deposit. See Appendix and Table A1 for details.

Method	Er. vol.[a] (km^3)	Er. mass[b] (kg)	DRE[c] (m^3)	Mag.[d]	Col.[e] (km)	Mean/Peak MDR (m^3/s)	Mean/Peak I.[f]
Exp. thinning	$9.69 \ 10^{-3}$	$7.36 \ 10^9$	$3.00 \ 10^6$	2.87	10.40	$2.92 \ 10^6$ / $1.36 \ 10^7$	9.47 / 10.1
Weibull	$2.37 \ 10^{-02}$	$1.80 \ 10^{10}$	$7.34 \ 10^6$	3.25	13.10	$7.14 \ 10^6$ / $3.33 \ 10^7$	9.85 / 10.5
Power Law	$1.27 \ 10^{-02}$	$9.63 \ 10^9$	$3.93 \ 10^6$	2.98	11.14	$3.82 \ 10^6$ / $1.78 \ 10^7$	9.58 / 10.3

Er. vol. = Erupted volume; Er. mass = Erupted mass; DRE = Dense Rock Equivalent volume; Mag. = Magnitude; Col. = Column height; Mean/Peak MDR = Mass Discharge Rate; Mean/Peak I. = Intensity.

a See Appendix for erupted volume parameters and method

b Deposit mass= Volume*Density taking a density equal to $760 \ kg/m^3$ (deposit density)

c DRE Volume= (Deposit mass)/(magma density) taking a magma density equal to $2450 - 2500 \ kg/m$ (andesite magma)

d Magnitude = log_{10}(deposit Mass)-7 (Pyle, 2000)

e Using the Sparks et al. (1997) model for a sustained plume, HT is related to the MDR (in this case, the mean MDR): $H_T = 0.220 \ MDR^{0,259}$

f Mean Intensity = log_{10}(Mean MDR) $+ 3$; Peak intensity = log_{10}(Peak MDR) $+ 3$ (modified from Pyle, 2000)

approximate values for channel widths and deposit thickness return bulk volume estimates of $\sim 1.2 \ 10^6$ m³, yet this is based on constant thicknesses extrapolated from final lobes and may be exaggerated.

3.3 Morphology of PDCs

Typically, sediment morphologies showed levees made of large clasts producing self-channelization with depleted inner channels in running parts, whereas lobes with tongue shapes developed at final local runout distances (Fig. 5-6). Interestingly, lobes could form even in very steep setting (>25° slope, *e.g.* Juive-viejo-minero Fig. 5d), whereas they could overrun long flat distances in other places (*e.g.* Pondoa). Two final lobes are found <1 m from a cliff and on a very inclined bed (Vascún and Juive-Viejo-minero, Fig. 5a and 5d). The Juive-Grande final lobe is found at almost right angle to the general slope and deviated in an artificial trench created to protect the main road from lahars, proving its efficiency for slow currents (Fig. 5c). PDCs travelling in the Hacienda valley were confined in a very narrow ravine (<10 m) were they could reach very low parts of the cone (Fig. 5e). They crossed the main road below the bridge without any damages. There, a lobe shape is scarred by a re-incision, the surface of the scar having a distinct color due to the absence of a final ash draping (Fig. 5e). At Achupashal the most distal deposits consists of two superposed PDC lobes of contrasting componentry and grain size distribution (Fig. 5f).

3.4 Temperature and disturbance from PDCs

Relatively low temperatures (40-170°C) were measured between 8 and 14 days after the eruption at depth down to 1 m in several valleys (Table 3). No pattern could be recognized in the temperatures regarding PDCs' observed chronology, componentry, or morphology. For all PDC deposits, even when no thermometer was available, a warm temperature was manually checked to ensure the primary and recent nature of the deposits.

In some areas close to the PDC pathways, vegetation was affected and found with dead leaves in the days to weeks following the eruption. This contrasted with early observations (1 day after eruption) documenting leaves covered by ash but not burnt (Yepes, pers. comm.). Zones on outer curves of PDCs pathways were affected with dead leaves on a much wider zone than in inner curves (Fig. 7). In the steep-sided, narrow valley of Juive-Pampa, PDCs got highly constrained in an edgy curve downstream a cliff (Fig. 7a-b). There, the outer valley sides were ploughed and scratched up to 15 m above the deposit surface during the flows, and young trees were unrooted or broken (Fig. 7c-d). Above, vegetation had dead leaves up to 60 m above the deposit surface on a very narrow zone (Fig. 7b). This corroborates with a video recording the growth of a co-PDC cloud at this location when flow fronts reached the zone (Diego C.F., Fig. 7a, 7e). Further, vegetation was affected in front of PDC lobes deposits up to 38 m in zones of high slope (*e.g.* Juive-Grande, Fig. 5c), but less than 1 m in flat terminal areas (*e.g.* Rea, Fig. 7f).

3.5 Stratigraphy and lithologic components

The composite stratigraphic column of tephra fall deposit consists in three recognizable layers (Fig. 8). Even when this full sequence is observed (*e.g.* at Palictahua, sample P1), the sequence remains incomplete in most outcrops. The basal layer (1) is a grayish to reddish fine-grained ash deposit (<1 mm in thickness. Above, layer 2 is thicker (1-8 mm) and formed by gray and coarse-grained ash deposits and lapilli sized fragments. Lapilli-sized, porphyric, andesite, dense and dark clasts (Fig. 8) are the most abundant (62.2-64.7 vol.%). They have sharp edges and contain crystals of Plagioclase (Pl) and Pyroxene

Figure 5. Picture of the final lobe in each valley: (a) Vascún (b) Juive-Pampa (c) Juive-Grande; note deviation by an artificial trench. (d) Juive-Viejo-minero; note cliff behind front, (e) Hacienda - The flow front continued through an inaccessible cliff; note the lobe scar, (f) Achupashal - Note two superposed lobes of contrasting content. (g) Achupashal-West (h) Romero proximal - photographed after first rain, (i) Romero distal lobe, (j) Rea (This lobe was not accessible so that the scale is not documented).

Figure 6. Surface observations of PDC deposits: (a) Levée made of large cauliflower clasts. (b) Variability of juvenile blocks encountered, with dense (top left), cauliflower (lower part), and bread crusted (top right) clasts. (c) A fines-depleted surface with large blocks vs. (d) A fines-rich surface with smaller blocks. Same pen for scale in each picture.

(Px). Dark-gray to reddish scoria fragments represents the second most abundant clast type (14.5-16.8 vol.%, Fig. 8). They are blocky, sub-rounded to sub-angular, with a vitreous matrix and high presence of non-elongated irregular-shaped vesicles. Light-to-gray pumice is also abundant (15.5-15.9 vol.%), being sub-angular in shape, with moderately microvesicular texture made of elongated to sub-spherical vesicles (<1 mm, Fig. 8). The matrix includes nailed Pl phenocrysts reaching 1 mm and minor presence of Px. This layer also contains a subordinate altered lithics fraction (5.5-5.9 vol.%, Fig. 8) and scarce volcanic glass (<1 vol.%, Fig. 8). Ultimately, the top layer (3) is very thin (<1 mm) and consists of Px and Pl crystals and abundant (>50%) juvenile volcanic glass (Fig. 8). It also comprises reddish, non-vesicular, dense altered fragments and white particle aggregates. The same type of samples were obtained in-situ (during the ash sedimentation over plane surfaces) at Pillate, after discrete explosions in mid-February 2014. At greater distances from the vent (*e.g.* Penipe, 14.3 km southwest), volcanic glass is a major component. It has a curviplanar surface and sharp morphology, in some cases of "shard" type, transparent to semi-
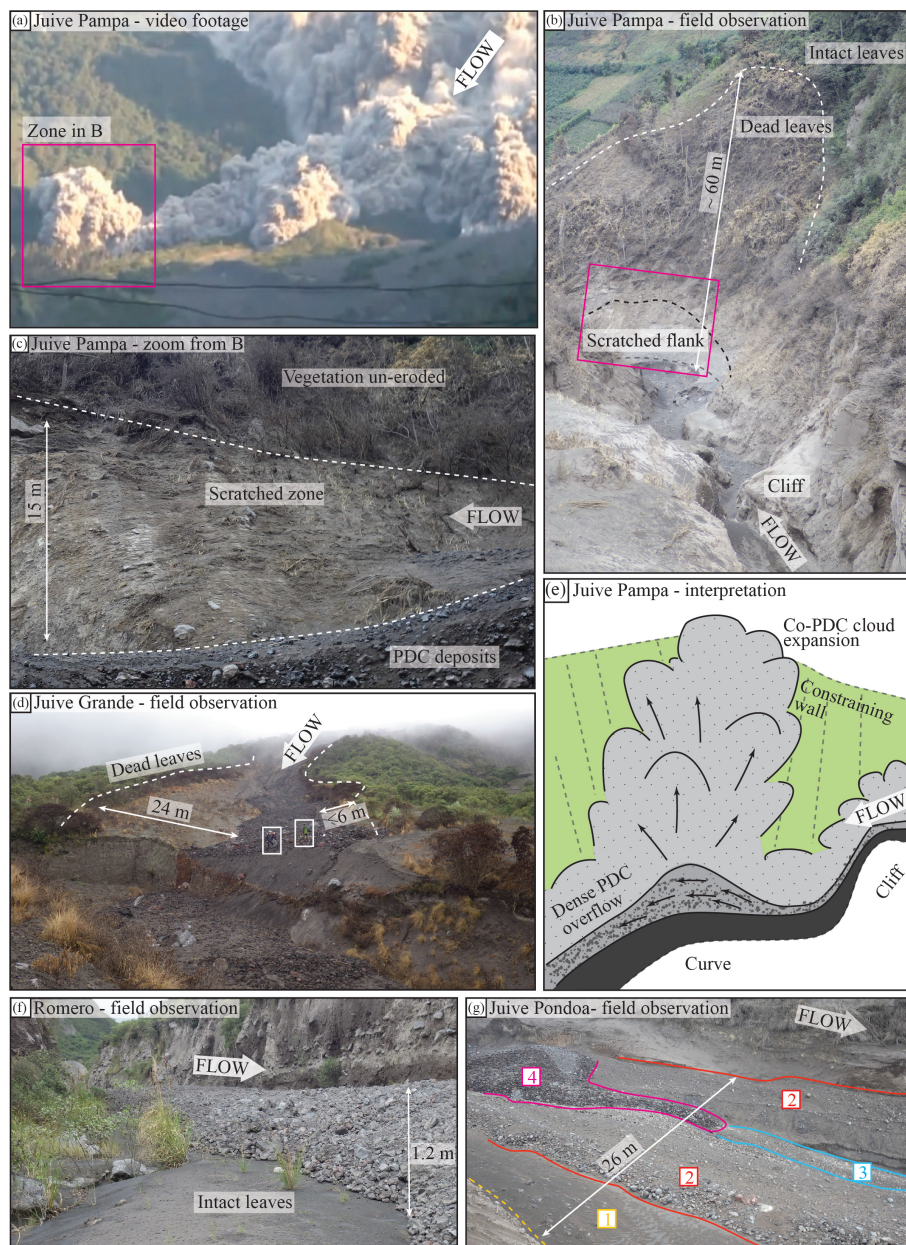
Figure 7. (a) Direct observation of PDCs during flow, youtube video (C.F. Diego). (b) Observation of PDCs' impacts in zone highlighted in (a), emphasizing dead leaves due to co-PDC clouds in a topographically highly constrained valley, downstream a cliff and on the outer overbank of a valley curve. (c) Zoom from B on the basal zone, note scratches. (d) The outer overbank of a valley curve shows no trees sideways from dense PDC deposits and damaged vegetation up to a distance of 24 m, whereas damaged vegetation is visible only 6 m sideway on the inner curve. (e) Interpretative sketch for (a)-(b)-(d). (f) Contrasting, leaves are still standing less than 1 m from PDCs in the lower Romero valley. (g) At least four successive units are recognized in the Juive drainage - Pondoa zone.

Table 3. Temperature profiles within final PDC deposit lobes.

Valley	J. Pampa-1		J. Grande		J. Pampa-2		J. Chontal		J. Pondoa-1		J. Pondoa-2		Achu.		Achu-W		Hacienda	
Date	08.02		08.02		09.02		09.02		10.02		10.02		14.02		14.02		14.02	
Data	D	T°	D	T°	D	T°	D	T°	D	T°	D	T°	D	T°	D	T°	D	T°
	50	128	45	84	5	43	50	52	55	65	5	35	45	43	40	62	30	39
	55	153	60	92	30	53	65	58	75	83	45	80	55	84	45	63	-	-
	65	158	95	99	50	86	90	58	100	102	90	107	60	70	60	81		
	70	171	100	97	70	105	-	-	-	-	105	95	65	76	-	-		
	-	-	-	-	80	120					-	-	-	-	-	-		

The date gives the measurement day, D: depth in centimetres, T°: temperature in °C.

transparent and black to clear-brown in color. It is accompanied by Pl free euhedral crystals (15 vol.%), in most cases fractured, and rounded to polygonal-shaped reddish altered fragments (25 vol.%).

The PDC deposits include blocks and bombs grouped in four types (Fig. 6b): 1) dense, seemingly-glassy (micro-cristalline) clasts with pervasive fracture pattern, 2) dark to greenish, porous, cauliflower-shaped, glassy clasts, 3) light-gray, micro vesicu-

5   lar, bread-crusted clasts with dense, fractured margins up to 3 cm thick, and 4) accidental lithics. According to Hall et al. (2015) the February eruption PDC deposits stratigraphy is segregated into a poorly-developed top layer compound by both sub-angular to sub-rounded clasts of black vesiculated andesite (juvenile andesite), as well as subordinate number of gray dense andesite clasts, and a fines-rich lower layer is dominated by dense andesite clasts whose angular clasts have micro-fractures and chilled margins. Whereas this sequence can occur in some areas, many flows can be superimposed in other zones (*e.g.* > 4 successive

10   units in Juive-Pondoa). Individual lobes show very variable aspect in terms of largest clast size, surficial fine content, and most frequent type of clast encountered (Fig. 6c-d). No tendency could be encountered with runout distance or eruption chronology. The superficial differences in content of fines is however absent in subsurface, where it seems constant between lobes with varying surface signatures. This suggests that the superficial content is a simple effect of local winds during emplacement. The size of the largest block fraction can vary from ca. 5 cm in some lobes to >40 cm in others (Fig. 6c-d).

15   **3.6   Grain size**

Four samples collected from tephra fall deposits were sieved for grain size analysis. Samples B1 and C1 show unimodal distribution, whereas C2 and SJ are bimodal and trimodal, respectively (Fig 9).

Sample B1 is composed of coarse to very fine ash (mode at 2.66 ϕ), with moderate sorting (according to the classification of Folk and Ward, 1957) or very well sorted (according to Cas and Wright, 1987) and with a coarse-skewed distribution.

20   Sample C1 is mostly made up of coarse ash (mode at 1 ϕ), showing the same sorting as B1, and very fine skewed distribution. Sample C2 is bimodal (1.5 and -1.0 ϕ) and it is mostly composed of of fine lapilli and coarse to medium sized ash, poorly
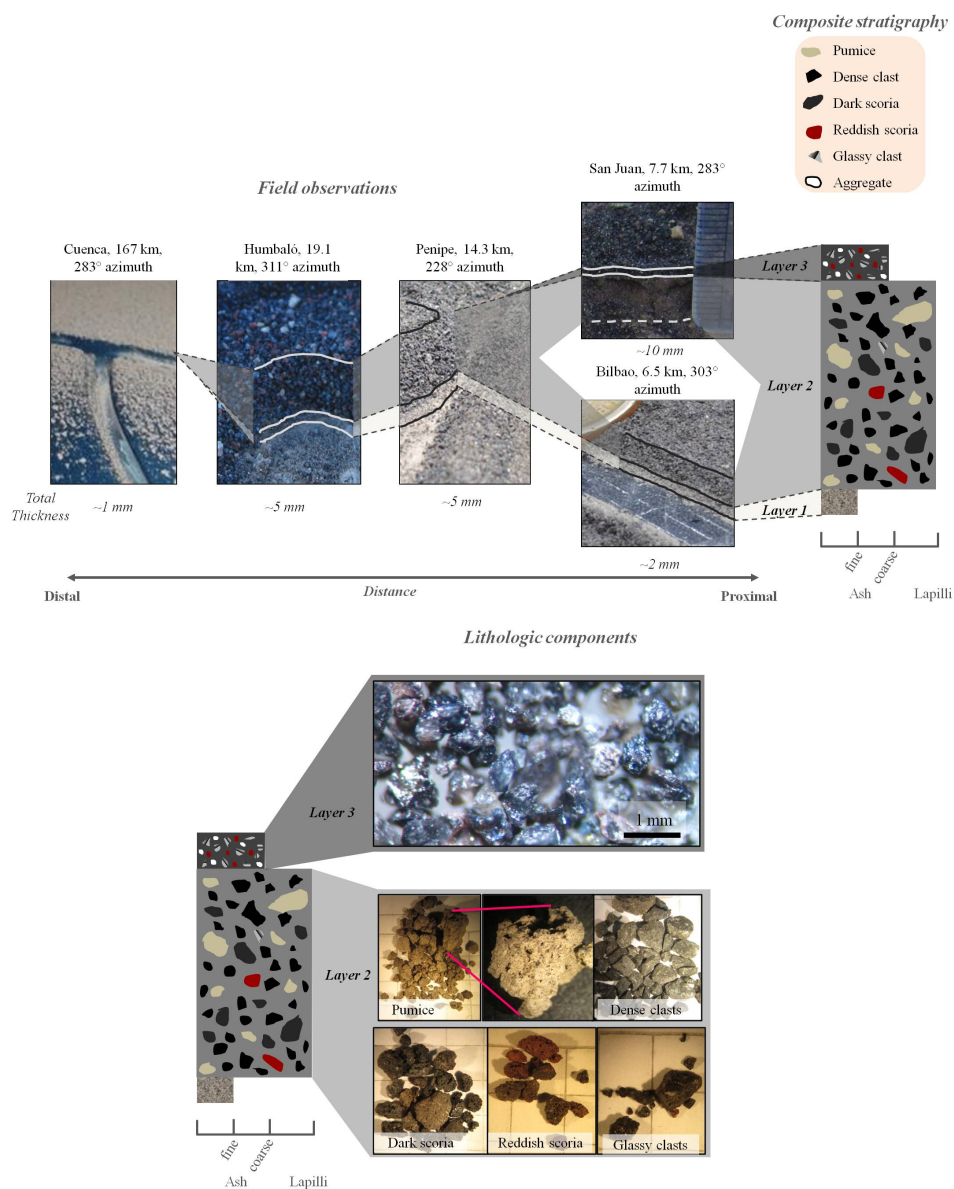
Figure 8. Field observations, stratigraphy and lithologic components of tephra fall deposits of the February 2014 eruption.

to well sorted (depending on the classification applied: Folk and Ward, 1957; Cas and Wright, 1987, respectively), and very coarse skewed.

Sample SJ has a singular trimodality (3.73, 2.5 and -2.16 ϕ). It contains a low amount (<15 wt.%) of coarse material (medium lapilli to coarse ash), a notable proportion (ca. 60 wt.%) of medium to fine ash, and less very fine ash (ca. 25 wt.%), being poorly sorted and coarse skewed. All the samples are leptokurtic (*i.e.* better sorted than a standard deviation).
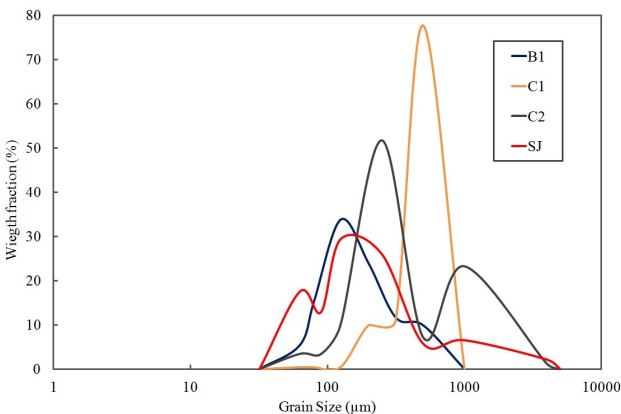

Figure 9. Grain-size analysis for samples from tephra fall collected around Tungurahua two weeks after eruption

Table 4. Grain size parameters for the tephra samples.

Samp	Lat (S) / Long (W) / Alt (m)	D (km)	Dir. (°)	Md	Mz	σ_1	Sk	KG	M1	M2	M3	Type	Sort.
P1	1°30'56" / 78°28'49" / 2434	6.36	219.1										
B1	1°24'0.4" / 78°25'7.5" / 1830	8.4	19.3	2.41	2.32	0.94	-0.2	1.12	2.66			U	MS
C1	1°32'53" / 78°29'44" / 2962	10.3	212.5	0.64	0.78	0.57	2.18	7.92	0.5			U	MWS
C2	1°32'47" / 78°29'49" / 2984	10.4	213	1.36	1.04	1.36	-0.4	2.46	1.5	-1		B	PS
SJ1	1°27'13" / 78°30'38" / 2447	7.4	283	1.36	1.04	1.36	-0.4	2.45	3.73	2.5	-2.16	T	PS

D: Direct distance from the crater, Dir: Orientation of crater-sample vector to the North, Md: median particle diameter, Mz: mean particle diameter, σ_1 : deposit sorting, Sk: deposit skewness, KG: Kurtosis, Modes (1, 2 and 3) are represented by M1, M2 and M3.

All grain size distribution values expressed in ϕ. Sample P1 was only analyzed for lithology.

U= Unimodal, B= Bimodal, T= Trimodal; MS= Moderately Sorted, MWS= Moderately well sorted, PS= Poorly sorted.

All samples from PDCs present a main mode at 125 μm (3 ϕ), with lesser secondary peaks at 250 (2 ϕ) and 500 μm (1 ϕ) (Fig. 10). Most samples follow a very consistent trend (black samples), with three samples slightly enriched in their fraction 125 and 90 μm (3.5 ϕ; cyan), yet this seems to only correspond to a minor measurement deviation and is not reflected in other fractions. Three samples have clearly distinct signatures switched towards the fines (red, blue, magenta). Two of these correspond to overflow sampling areas from co-PDC clouds rather than dense PDCs deposits (Romero T104 and Pampa T10).

The third fine-grained sample (blue, Pondoa T110, coord. N0782730; E9842149) was collected on the lowermost deposit of a zone with at least four discrete PDC pulses at Juive Pondoa valley (Fig. 7g). In terms of median diameter vs sorting, the dense PDCs samples plot in the field of "flow" evidenced by Walker (1971), whereas the samples from co-PDC clouds and Pondoa overlap the "surge" field (Fig. 10e).
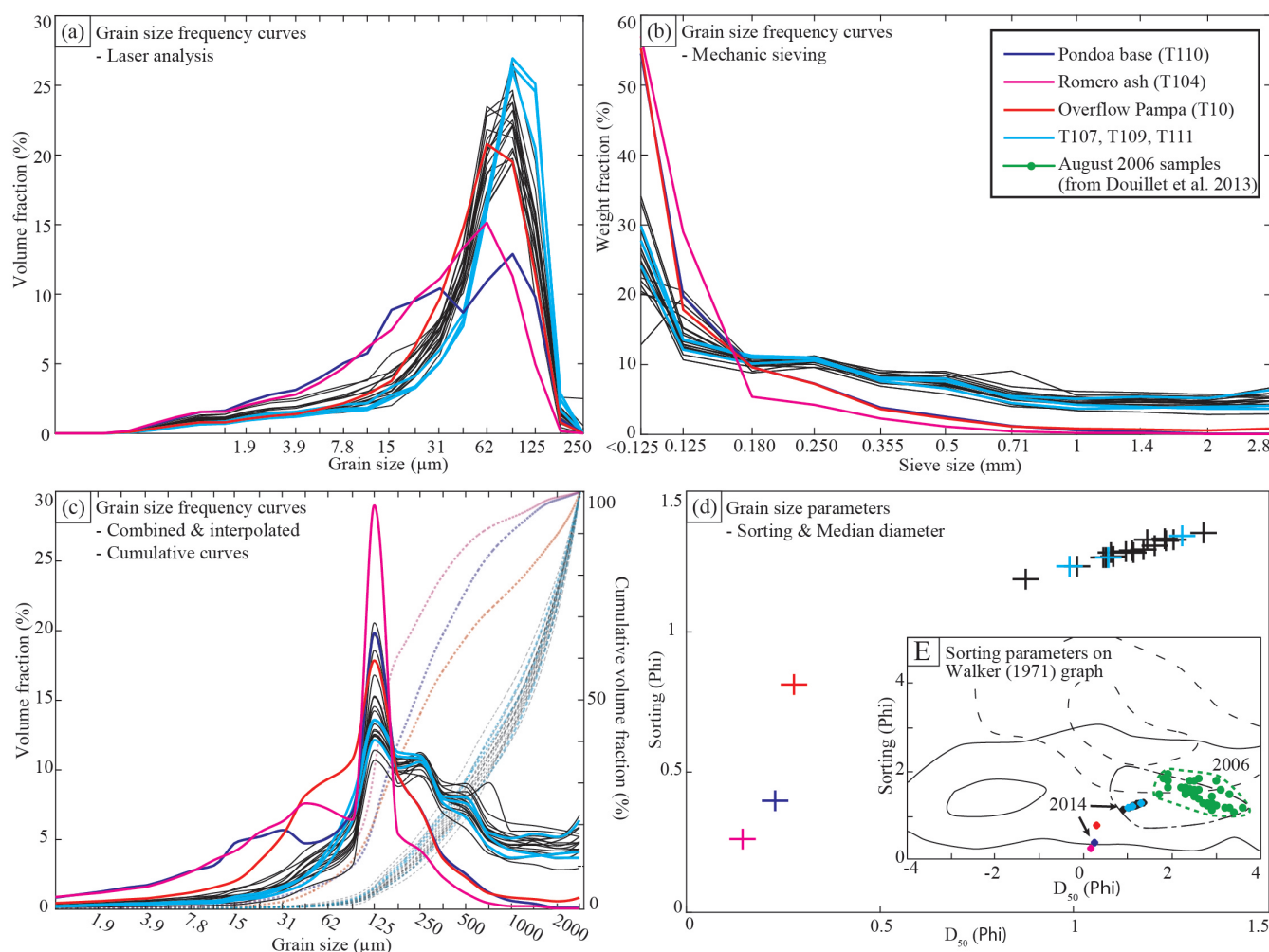

Figure 10. Grain-size analysis for samples from PDC deposits. Frequency curves for (a) laser and (b) mechanic sieving. (c) Combined and interpolated curves from (a)-(b) (full lines, left scale) with cumulative curves (dashed lines right scale). (d) Sorting and median diameters calculated from the cumulative curves with the flow (dashed) vs. fall (plain) vs. surge (dotted) fields from Walker (1971) in background and comparison with dilute PDCs from the August 2006 eruption. Anecdotic samples are marked in colors.
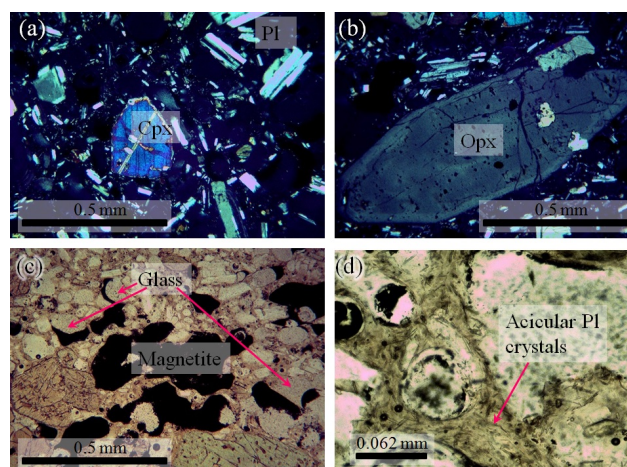
Figure 11. Texture and mineral assemblage of a juvenile, low density scoria bomb revealed by optical microscope. The mineral assemblage consist of plagioclase (Pl), clinopyroxene (Cpx) and orthopyroxene (Opx) crystals, as seen in cross-polarized light (a and b). (c) Magnetite and volcanic glass vesicles observed in plane polarized light. (d) Cryptocrystalline groundmass with acicular Pl crystals observed in plane polarized light.

3.7 Petrography and geochemistry

Thin sections were obtained from a juvenile cauliflower bomb. It is a dark porphyric (16% phenocrysts) and faint trachytic andesites with profuse vesiculation (Fig. 11). The mineral assemblage is different to that observed in 2006 eruption products (Samaniego et al., 2011) and consists mostly of subhedral and prismatic Pl phenocrysts (17%), Cpx (10%) and Opx (2%). Pl

5　crystals show polysynthetic twins and clear zonation, and include euhedral to subhedral zircons. Euhedral to subhedral Cpx show zoned rims and appear as single phenocrysts or as agglomerated rounded crystals. The Opx and Cpx glomeroporphydic textures are occasionally present. The matrix consists of magnetite and glass vesicles (25 and 31% respectively), plus Pl small acicular crystals (17%) in a cryptocrystalline groundmass (Fig. 11c). Preliminary XRF analysis show that the black vesicular juvenile scoria correspond to a medium-K (1.55 wt.%) andesite (59.4 wt.% of SiO_2) composition, very similar to composi-

10　tions of previous eruptions (*e.g.* July 2013, August 2006). According to traditional classification schemes of igneous rocks from Le Maitre et al. (1989) and Shand (1949), this sample is included in the Calc-alkaline series and presents peraluminous composition, respectively.

4 Discussion

4.1 Data reliability

As a direct consequence of fast reworking of tephra, only 23 sites were measured, and this, only in proximal areas where erosion did not affect the deposits. Further, field work was carried out 2-3 weeks after the eruption's onset, and tephra samples

5 thus contain the signature from the paroxysm event of 01 February, but also from the two weeks of subsequent lower intensity Strombolian activity. However, the tephra cloud accompanying the paroxysm propagated in a very unusual S-SW direction whereas the tephra clouds from the post-paroxysm activity followed the usual cloud-pathway aligned with the westward wind direction. The signal thus seems to be largely the one from the main eruption due to the S-SW elongated shape of the isopachs. The amount of tephra identified as deposited by the subsequent activity (02-14 February) represents less than 1 mm in proximal

10 areas along the dispersal axis produced by discrete, sporadic low intensity explosions.

Depending on the number and distribution of data points, uncertainty in the isopach areas ranges between 7 to 30%, and can be even larger in intermediate and proximal zones (Klawonn et al., 2014). Here, most of the measurements are restricted to <15 km radius from the vent, and they are, in general >0.5 cm in thickness. Thus, the lack of measurements in distal areas may produce a considerable uncertainty (30%). Bernard et al. (2013) suggested that the amorphous (non-elliptical) shape of

15 isopachs/isomass curves produced by wind direction variability and subjective reconstruction of these curves, was an important factor in the error estimation during 2012-2013 Tungurahua eruptions. We do not expect high uncertainty related to the tephra fall distribution shape for this study case, since the wind direction of the 01 February event produced nearly elliptical isopachs. In terms of the grain size measurements for the eruption, they are scarce, and the lack of data results in a restricted range of distributions which is not sufficient to assess a total grain size distribution.

20 4.2 Origin of fallout deposits

The three tephra fall layers have distinct signatures that allow their correlation to different events.

Layer 1, with a basal stratigraphic position, whitish/reddish fine-grained ash content and location near the vent is atypic and can be correlated by color to the eruption of 14 July 2013, as interpreted by Hall et al. (2015). Layer 2 is the thickest layer, and contains the S-SW elongated isopach signature. It thus most likely represents the 01 February 2014 eruption. The abundant

25 porphyric, dense and dark andesite lapilli are interpreted to belong to a recent event, yet not the 01 February 2014 eruption. In that sense, they represent lithics. Their abundance and minor presence of vesicular juvenile pumice and dark scoria in layer 2 may indicate an eruptive mechanism triggered by gas accumulation, with destruction of a plug/conduit walls(*e.g.*, Morrissey and Mastin, 2000). The elongated/rounded morphology and bubbly/glassy texture of juvenile pumice has been interpreted by Polacci (2005) as representative of the central part of a magmatic column at the conduit during Plinian eruptions, where vesicles

30 are free to grow and only subjected to elongational stresses. They may be broken pieces of the blocks with cauliflower and bread crust textures encountered in the PDC deposits. This texture has been associated to blocks released by Vulcanian eruptions (*e.g.*, Wright et al., 2007). The existence of low amounts of altered lithics may be interpreted as the erosion of conduit's wall erosion during the transition from Vulcanian to Strombolian style. A shallow dynamism of conduit destabilization, syn-

eruptive decompression and magma fragmentation, conduit emptying and expulsion of juvenile pumice (Gottsmann et al., 2011) is suggested by the tephra components of layer 2. Contrasting, layer 3 presents high amount of volcanic glass together with abundant altered lithics, which are characteristic for a fully open-vent system with Strombolian activity. This would have eroded the upper conduit and transported large amounts of juvenile fragments, in this case represented by volcanic glass and free crystals.

4.3 PDC material

The low temperatures measured at PDC lobe deposits are striking in comparison with the simultaneous occurrence of carbonized wood fragments. This can be explained by the fact that there was only a low component of hot juveniles. Wood in contact with hot juvenile was carbonized, yet there was not enough of these clasts to make the whole deposit hot. The dense plug fragments were probably relatively cold. There was further probably also a lot of flow bulking, *i.e.* entrainment of cold clasts, as suggested for previous events by Bernard et al. (2014). A large part of the material that could be interpreted as fresh juvenile probably corresponds to material ejected during preceding small events from the previous year. This material accumulated in the upper flanks would have been destabilized during the 01 February explosions and help to trigger the formation of PDCs. Thus, even if a relatively small eruption occurs, it can lead to formation of PDCs if material has previously accumulated without stabilization on the upper flanks during preceding events.

The variability in the amount of ash visible at the surface of the PDC deposits was previously interpreted as representing two stages of the eruption. Although there may be more fines in basal units compared to the top layer in some particular cases, this is not systematic at all, and seems to be due to wind during emplacement rather than reflecting the eruptive dynamics. This is further supported by the video footage of the eruption showing that co-PDC clouds were rapidly drifted by the wind in some ravines (C.F. Diego, youtube). Sample T110 from the basal layer of Pondoa zone illustrates this further, since this PDC deposit surface was covered by at least 3 further co-PDC clouds, and thus has a co-PDC cloud signature in its superficial grain size.

The variability in componentry and aspect of the final lobes and channels might have a signature from the eruption dynamics, yet the first emitted flows remained deposited on the proximal Achupashal drainage, and were likely re-entrained during the main-PDC flows. It seems that the Vascún and Juive drainage flows have more dense fractured blocks whereas the western deposits are richer in cauliflower and altered clasts. This would go against the eruption dynamics chronology with initial plug destruction, since the first PDCs were emitted in the proximal Achupashal, and then the onset of the third explosion triggered PDCs in the SW ravines (Rea and Romero), and later in the Vascún, Juive, lower Achuapashal and Hacienda almost simultaneously (Fig. 4).

No correlation of the grain-size curves with runout distance, componentry and morphology was observed, neither to any path-dependent abrasion and thus the grain size signature seems inherited from conduit fragmentation only. Two patterns are found from the grain size data. The "dense PDC" pattern is fairly homogeneous, and no trend was identified. It plots close to the fields of "dilute PDCs" from the 2006 eruption of Tungurahua (Douillet et al., 2013b, Fig. 10e). The "co-PDC cloud" pattern has more variability, and plots at the limit of the "fall" field of Walker (1971). Thus, the grain size is mainly a result of the transport process, dominated by elutriation from the dense PDCs and subsequent suspended transport.

It is noteworthy that neither the characteristics of the PDC deposits nor the thermal and color videos from the monitoring network (www.ig-epn.edu.ec) show any presence of lateral blast. Contrarily to Hall et al. (2015), we rather interpret the origin of the PDCs as a result of flank loading from a vertically erupting column, and subsequent destabilization of the material accumulated on the steep upper flanks, a mechanism quite similar to the 2006 PDCs (*e.g.* Kelfoun et al., 2009).

5   Volume calculations of PDCs and incandescent bombs over the flanks of the volcano estimated by Hall et al. (2015) are about $5.7 \ 10^6$ m^3. These measurements seem to be overestimated since they consider thicknesses at lower (thicker) emplacement areas. In facts, the thickness of the PDC deposits for the 2014 eruption is fairly unequal. Most of the material seems to be accumulated in discrete places and terminal lobes, but the majority of the pathway ravines were almost empty of PDC deposits, and only had levees, some even showed signs of erosion (and thus flow bulking). Field work was carried out before any rain

10   occurred, and thus there was no secondary transport by lahars. The first implication is that previously extrapolated PDC volume based on the thickness of terminal lobes is probably fairly exaggerated.

Most importantly, the February 2014 PDCs illustrate a new danger of the ongoing eruption: even with a small volume, PDCs are able to travel further and further. This character is likely due to the fact that ravines have been stripped and eroded by 15 years of lahars and PDCs. There are no more obstacles to PDCs' flow, no trees or natural dams. Thus even of small volumes,

15   future PDCs at Tungurahua are likely to reach the lower inhabited areas both easier (more frequently) and faster.

4.4 A plug-driven onset evolving into an open conduit eruption

Presence of disequilibrium textures in Pl (complex zoning patterns and resorption features) are usually interpreted as changing physical conditions in magmatic systems due to rapid decompression and/or magma mixing/mingling adding heat or mass (Nelson and Montana, 1992). The phenocrystal assemblage of the February eruption samples consisting in Pl and Px represents

20   the liquidus phases in equilibrium with the melt. As no reaction or disequilibrium textures were found, a rapid rise in liquid and crystals is required, in contrast to the 2006 eruption, where clear disequilibrium textures have been documented in Pl and Cpx phenocrysts (Samaniego et al., 2011). This scenario implies that the February magma was not re-heated or mixed. At the ejection level, a quick quenching process, rock fracturing and eruption is able to generate these andesite blocks and bombs included in the PDCs, without any evidence of interaction between two melts inside the magmatic reservoir. The geophysical

25   background of inflation (Vallejo et al., 2014) and striking seismicity 48 h before the eruption onset are probably triggered by the pressurization of the upper chamber due to the presence of a plug in the conduit (Fig. 12a). This rapidly evolved into a volcanic unrest and eruption. According to the direct observations of the eruption, we can infer that the plug failure was progressive, starting with the first explosion at 22:12 UTC (Fig. 12b) and then evolving into a total plug destruction at 22:39 UTC (Fig. 12c) during the paroxysmal phase of explosive activity. This Vulcanian mechanism is also supported by the componentry of tephra

30   fallout, and has already been described for previous eruptions at Tungurahua (*e.g.* Bustillos et al., 2016; Parra et al., 2016). After this phase, the componentry of Layer 3 indicates an eruptive style transition into an open-vent mechanism of Strombolian style, which is also supported by the direct observations (Fig. 12d). The geochemistry of the sample analyzed is in agreement with the composition of the products during the ongoing phase of Tungurahua (1999-2010), which mostly consist of andesites (58-59 wt.% of SiO_2, Samaniego et al., 2011; Myers et al., 2014). Even if there is general consensus in the mixing of a

volatile-rich basaltic andesite with a degassed andesite magma during the eruption of 2006 (Samaniego et al., 2011) Myers et al. 2014), the composition remains strikingly stable in the last fifteen years (1999-2014) of eruptions without notable changes in the feeding magma.
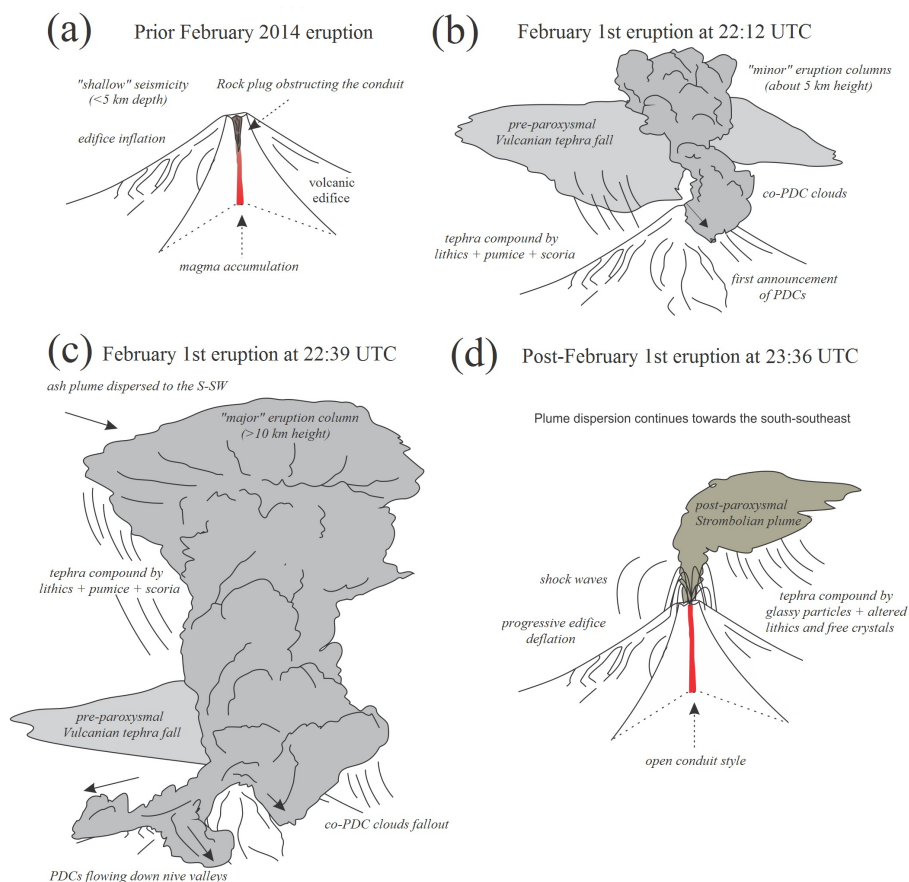

Figure 12. Dynamics of the February 2014 eruption at Tungurahua. (a) Pre-eruptive condition interpreted as plugging of the upper conduit. Fluid circulation cause alteration in the wall rock. The ascent of magma generates edifice inflation, and seismicity occurs only briefly before plug destruction due to faulting by overpressure. (b) The partial opening of the system generates small Vulcanian explosions and PDCs. (c) A major Vulcanian eruption with formation of a Subplinian column results from the total failure of the plug. PDCs descend the valleys on the flanks, transporting plug blocks, juvenile bombs and previously erupted material. (d) After the explosive paroxysm ends, the depressurization of the volcano causes deflation and activity continues with an open-vent system with Strombolian activity. The juvenile magma is released with scarce content of lithics.

Solid Earth

Discussions

Open Access

EGU

4.5 Volume and style

We suggest the Weibull volume calculation (Bonadonna and Costa, 2012) as the most realistic, due to its smaller mean relative squared error ($\sim$0.065) if compared to the other methods (Table 2). This method gives a volume estimate of $1.53 \ 10^7 \pm 0.35 \ 10^7 \ m^3$.
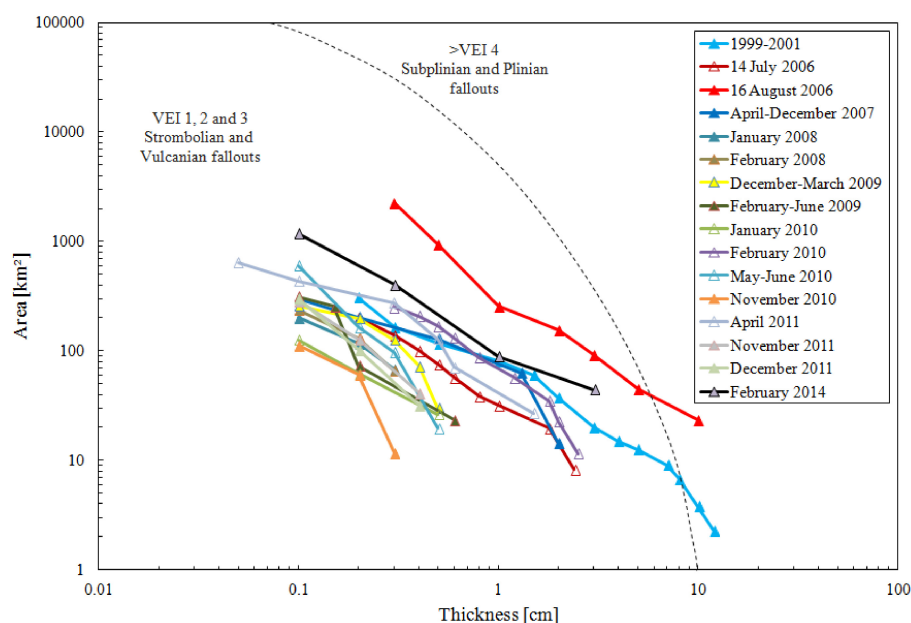

Figure 13. Plot of thickness vs. square root area for tephra fall deposits from eruptions during the period 1999-2014 at Tungurahua volcano (Modified from Bustillos et al., 2016).

5   Direct observations of the eruption columns of the paroxysmal event and the volume resulting from the integration of the fallout deposit isopachs allows estimation of the Mass Discharge Rate (MDR). We obtained a range of MDR values associated to the mean and peak eruption duration of 42 and 9 minutes (Table 2). Following the physical model of eruptive column in Sparks et al. (1997), the maximum column height (HT) would range from 10.4 to 13.1 km in height above the crater (Table A1), in agreement with the height reported by the VAAC (14 km a.s.l.).

10 Respective Magnitude and Intensity calculated following Pyle (2000) yield $\sim$3 and 9.5-11.0 (Table 2). The released tephra volume and maximum eruptive column height are consistent with a Volcanic Explosivity Index (VEI) of 3 (Newhall and Self, 1982). The column height and intensity suggest that peak activity resulted in a small Subplinian eruption (in the Cioni et al., 2015, classification). In contrast, the components of tephra deposits reflect a Vulcanian style. The deposits of the February 2014 eruption are similar to the 14 July 2006 eruption in terms of erupted tephra volume, and smaller than the 16 August 2006 major

15 event (Fig. 13), being the second largest tephra fall blanket deposited and mapped at Tungurahua between its reawakening in

1999 and 2016. If compared to the 14 July 2013 (2×10^{-4} km^3; Parra et al., 2016)) the 01 February 2014 eruption is $\sim$82 times larger.

4.6 Comparison with the 04 April 2014 eruption

An eruption with similar characteristics to that of 01 February 2014 occurred later on the 04 April 2014. The activity was preceded by a deformation pattern starting on 20 March 2014, followed by a sudden increase in the seismic activity less than 24 h prior to the eruption onset (55 VTs, 70 LPs and 5 tremor events Instituto Geofísico, 2014e). The eruption consisted of two explosive events, which produced an eruption column reaching 10 km a.c.l. and whose tephra was dispersed to the SW. The first explosion lasted 5 minutes and discharged PDCs which flowed down the Vascún and La Pirámide streams, while the second explosion started at 23:16 UTC and lasted 4 min. Tephra fall consisting mostly of lapilli-sized particles was reported at the towns of Bilbao, Choglontús, Chacauco and Cusúa ($<$10 km from the vent). Subsequently, the activity evolved into Strombolian explosions and a lava flow was emitted on 10 April 2014. The ash emissions continued several days after the lava effusion.

Although the tephra fall deposit has not been sampled in the current investigation, we suspect that the mechanism of the 04 April 2014 eruption was roughly similar to that shown by the 01 February 2014, based on the event sequence and short-lived unrest period. A value of 2.51×10^7 kg/s MDR is obtained for the HT column of the April eruption with the Sparks and Walker (1977) equation. Applying this MDR for an eruption duration of 9 minutes yields a total erupted mass of 1.36×10^9 kg, which represents between 9 and 14% of the total mass released during the February eruption studied here. Although the April eruption was smaller in size, the repeated Vulcanian mechanism with little warning observed at Tungurahua requires to be assessed because it augurs little forecast timing.

5 Conclusions

Based on field studies, laboratory analysis and eruption chronology, the February 2014 eruption of Tungurahua volcano corresponded to a moderate eruption of Vulcanian style, VEI 3. This is the second largest eruption at Tungurahua since the awakening in 1999, after the August 2006 event, with occurrence of PDCs reaching the base of the volcano.

Similarly to the 14 July 2013 eruption, the 01 February 2014 eruption of Tungurahua volcano showed several specificities in comparison with the traditional scheme of events from the 1999-2013 eruptive period, which urges for new tactics for risk prevention. Although the second largest since 1999 in terms of erupted volume and intensity, the onset of explosions and paroxysm were preceded by a very short period of seismic unrest, a characteristic shared with the later April 2014 eruption. The eruption and its short-lived unrest may be attributed to the presence of a rock cap (plug) in the conduit representing a future forecasting challenge.

The eruption can be summarized in two stages: 1) The onset of a striking seismic swarm of VT and LP events, associated with shallow processes of rapid unrest due to the failure of a rock plug (represented by the lithics in tephra layer 2). Petrography suggests the absence of interaction between juvenile andesite magma and host mush in the magma reservoir, in a quick process

of ascent, rise in pressure and trigger of the eruption process. This rules out magma mixing for this eruption. 2) A transition to Strombolian activity, evidenced by the increase of juvenile scoria in tephra fallout. The components of volcanic glass and altered lithics further suggest an open conduit dynamism, supported by the reduction of VT and LP seismicity in favor of harmonic tremors after the paroxysmal phase.

5   While most of the eruptive plumes from the 1999 to 2015 period dispersed tephra toward the W (Bustillos et al., 2016), the eruptive plume for the 01 February 2014 paroxysm was directed to the S-SW. This is explained by the fact that this eruption is the first large one affected by a very infrequent wind direction striking South. Future tephra fall hazard mitigation will need to account for this possibility.

     In terms of PDC hazard, the 01 February 2014 eruption showed that even small volumes of erupted material can produce

10 significant PDCs via flow bulking through material erupted from preceding events on the upper flanks. The ravines that have been stripped by 15 years of eruption further increase hazard, since flows are free to flow down faster and further than they would in a vegetated and naturally damned ravine.

     The 01 February 2014 eruption signed the evolution of the eruptive style of Tungurahua from a Subplinian to a Vulcanian-dominated eruptive behavior. The short warning preceding the eruption, followed by occurrence of PDCs reaching inhabited

15 areas, together with the large amount of fallout erupted and dispersed toward a very infrequent direction represent a high hazard. This event thus urges for revised hazard mitigation scenarios at Tungurahua and can serve as an example for other volcanoes in crisis.

Appendix A: Calculation of erupted parameters

Table 2 gives the results of calculation following three interpolation methods, with details below and used parameters in

25 Table A1:

-Exponential thinning volume is calculated through the adjunction of the volumes calculated for the Segments 1 and 2 following the method of Pyle (1989): $V = c * e^{(-mx)}$

     -Weibull method used the Weibull function integration (Bonadonna and Costa, 2012): $V = 2((\Theta * \lambda^2)/\eta)$

     -Power law is following the approach of Bonadonna and Houghton (2005). TPL and m are coefficient and exponent of the

30 power law. Here, we used as C=2 and B=600 as both proximal and distal limit of integration: $T(x) = T_{pl} * A^{(-0.5m)}$;

$V = [2T_{pl}/(2 - m)] * [C^{(2-m)} - B^{(2-m)}]$

Solid Earth
Discussions
Open Access
EGU

Table A1. Volume and mass calculation for the tephra fall deposit.

Method	Parameter	Total deposit (Layers 1+2+3)
Exponential thinning	number of isopachs	6
	mean rel. squared error	0.05074
	Segment 1 (km^3)	$4.71 \ 10^{-3}$
	$c1$	0.06283
	$m1$	0.1555
	Segment 2 (km^3)	$4.98 \ 10^{-3}$
	$c2$	$2.504 \ 10^{-3}$
	$m2$	$28.91 \ 10^{-3}$
Weibull method	number of isopachs	6
	mean rel. squared error	0.01782
	Θ	0.0003547
	λ	99.69
	η	0.2979
Power Law	number of isopachs	6
	mean rel. squared error	0.01832
	PL-coefficient (TPL)	0.9625
	PL-Exponent (m)	1.931
	Estimated proximal limit	4.109

5   *Competing interests.* None

Disclaimer. TEXT

References

Arellano, S., Hall, M., Samaniego, P., Le Pennec, J.-L., Ruiz, A., Molina, I., and Yepes, H.: Degassing patterns of Tungurahua volcano (Ecuador) during the 1999–2006 eruptive period, inferred from remote spectroscopic measurements of SO 2 emissions, Journal of Vol-
5   canology and Geothermal Research, 176, 151–162, 2008.

Bernard, B., Bustillos, J., Wade, B., and Hidalgo, S.: Influence of the wind direction variability on the quantification of tephra fallouts: December 2012 and March 2013 Tungurahua eruptions, Avances, 5, A14–A21, 2013.

Bernard, J., Kelfoun, K., Le Pennec, J.-L., and Vargas, S. V.: Pyroclastic flow erosion and bulking processes: comparing field-based vs. modeling results at Tungurahua volcano, Ecuador, Bulletin of Volcanology, 76, 1–16, 2014.

10   Bernard, J., Eychenne, J., Le Pennec, J.-L., and Narváez, D.: Mass budget partitioning during explosive eruptions: insights from the 2006 paroxysm of Tungurahua volcano, Ecuador, Geochemistry, Geophysics, Geosystems, 17, 3224–3240, 2016.

Blott, S. J. and Pye, K.: GRADISTAT: a grain size distribution and statistics package for the analysis of unconsolidated sediments, Earth surface processes and Landforms, 26, 1237–1248, 2001.

Bonadonna, C. and Costa, A.: Estimating the volume of tephra deposits: a new simple strategy, Geology, pp. G32 769–1, 2012.

15   Bonadonna, C. and Houghton, B.: Total grain-size distribution and volume of tephra-fall deposits, Bulletin of Volcanology, 67, 441–456, 2005.

Brown, R. J. and Andrews, G.: Deposits Of Pyroclastic Density Currents, in: The encyclopedia of volcanoes, edited by Sigurdsson, H., Houghton, B., McNutt, S., Rymer, H., and J, S., chap. 35, pp. 631–648, Elsevier, 2015.

Bustillos, J.: Transition de style éruptif au cours des éruptions andésitiques en système ouvert: apport de l'étude des cendres avec application
20   au volcan Tungurahua (Equateur). MSc. Thesis, Université Nice Sophia Antipolis, 2010.

Bustillos, J., Romero, J. E. J. E., and Troncoso, L.: Tephra fall at Tungurahua Volcano (Ecuador)–1999-2014: An Example of Tephra Accumulation from a Long-lasting Eruptive Cycle, Geofísica internacional, 55, 55–67, 2016.

Cas, R. and Wright, J.: Volcanic Successions, Modern and Ancient: A Geological Approach to Processes, Products and Successions, 528 pp, 1987.

25   Champenois, J., Pinel, V., Baize, S., Audin, L., Jomard, H., Hooper, A., Alvarado, A., and Yepes, H.: Large-scale inflation of Tungurahua volcano (Ecuador) revealed by Persistent Scatterers SAR interferometry, Geophysical Research Letters, 41, 5821–5828, 2014.

Cioni, R., Pistolesi, M., and Rosi, M.: Plinian and Subplinian eruptions, in: The encyclopedia of volcanoes, edited by Sigurdsson, H., Houghton, B., McNutt, S., Rymer, H., and J, S., chap. 29, pp. 519–536, Elsevier, 2015.

Clarke, A., Ongaro, T., and Belousov, A.: Vulcanian eruptions, in: The encyclopedia of volcanoes, edited by Sigurdsson, H., Houghton, B.,
30   McNutt, S., Rymer, H., and J, S., chap. 28, pp. 505–518, Elsevier, 2015.

Cole, P., Stinton, A., Odbert, H., Bonadonna, C., and Stewart, R.: An inclined Vulcanian explosion and associated products, Journal of the Geological Society, 172, 287–293, 2015.

Douillet, G. A., Pacheco, D. A., Kueppers, U., Letort, J., Tsang-Hin-Sun, È., Bustillos, J., Hall, M., Ramón, P., and Dingwell, D. B.: Dune bedforms produced by dilute pyroclastic density currents from the August 2006 eruption of Tungurahua volcano, Ecuador, Bulletin of
35   Volcanology, 75, 1–20, 2013a.

Douillet, G. A., Tsang-Hin-Sun, È., Kueppers, U., Letort, J., Pacheco, D. A., Goldstein, F., Von Aulock, F., Lavallée, Y., Hanson, J. B., Bustillos, J., et al.: Sedimentology and geomorphology of the deposits from the August 2006 pyroclastic density currents at Tungurahua volcano, Ecuador, Bulletin of Volcanology, 75, 1–21, 2013b.

Solid Earth
Discussions

Open Access

EGU

Eychenne, J., Le Pennec, J.-L., Troncoso, L., Gouhier, M., and Nedelec, J.-M.: Causes and consequences of bimodal grain-size distribution of tephra fall deposited during the August 2006 Tungurahua eruption (Ecuador), Bulletin of Volcanology, 74, 187–205, 2012.

Eychenne, J., Le Pennec, J.-L., Ramón, P., and Yepes, H.: Dynamics of explosive paroxysms at open-vent andesitic systems: high-resolution mass distribution analyses of the 2006 Tungurahua fall deposit (Ecuador), Earth and Planetary Science Letters, 361, 343–355, 2013.

Fierstein, J. and Nathenson, M.: Another look at the calculation of fallout tephra volumes, Bulletin of Volcanology, 54, 156–167, 1992.

Folk, R. L. and Ward, W. C.: Brazos River bar: a study in the significance of grain size parameters, Journal of Sedimentary Research, 27, 1957.

Gottsmann, J., De Angelis, S., Fournier, N., Van Camp, M., Sacks, S., Linde, A., and Ripepe, M.: On the geophysical fingerprint of Vulcanian explosions, Earth and Planetary Science Letters, 306, 98–104, 2011.

Hall, M. L., Robin, C., Beate, B., Mothes, P., and Monzier, M.: Tungurahua Volcano, Ecuador: structure, eruptive history and hazards, Journal of Volcanology and Geothermal Research, 91, 1–21, 1999.

Hall, M. L., Steele, A. L., Mothes, P. A., and Ruiz, M. C.: Pyroclastic density currents (PDC) of the 16–17 August 2006 eruptions of Tungurahua volcano, Ecuador: Geophysical registry and characteristics, Journal of Volcanology and Geothermal Research, 265, 78–93, 2013.

Hall, M. L., Steele, A. L., Bernard, B., Mothes, P. A., Vallejo, S. X., Douillet, G. A., Ramón, P. A., Aguaiza, S. X., and Ruiz, M. C.: Sequential plug formation, disintegration by Vulcanian explosions, and the generation of granular Pyroclastic Density Currents at Tungurahua volcano (2013–2014), Ecuador, Journal of Volcanology and Geothermal Research, 306, 90–103, 2015.

Hidalgo, S., Battaglia, J., Arellano, S., Steele, A., Bernard, B., Bourquin, J., Galle, B., Arrais, S., and Vásconez, F.: SO$_2$ degassing at Tungurahua volcano (Ecuador) between 2007 and 2013: transition from continuous to episodic activity, Journal of Volcanology and Geothermal Research, 298, 1–14, 2015.

Inman, D. L.: Measures for describing the size distribution of sediments, Journal of Sedimentary Research, 22, 1952.

Instituto Geofísico, E. P. N.: Informe especial del volcán Tungurahua no. 01, http://www.igepn.edu.ec/, accessed: 2014-02-09, 2014a.

Instituto Geofísico, E. P. N.: Informe especial del volcán Tungurahua no. 02, http://www.igepn.edu.ec/, accessed: 2014-02-09, 2014b.

Instituto Geofísico, E. P. N.: Informe especial del volcán Tungurahua no. 04, http://www.igepn.edu.ec/, accessed: 2014-02-09, 2014c.

Instituto Geofísico, E. P. N.: Informe especial del volcán Tungurahua no. 05, http://www.igepn.edu.ec/, accessed: 2014-02-09, 2014d.

Instituto Geofísico, E. P. N.: Informe especial del volcán Tungurahua no. 07, http://www.igepn.edu.ec/, accessed: 2014-05-13, 2014e.

Kelfoun, K., Samaniego, P., Palacios, P., and Barba, D.: Testing the suitability of frictional behaviour for pyroclastic flow simulation by comparison with a well-constrained eruption at Tungurahua volcano (Ecuador), Bulletin of volcanology, 71, 1057–1075, 2009.

Klawonn, M., Houghton, B. F., Swanson, D. A., Fagents, S. A., Wessel, P., and Wolfe, C. J.: From field data to volumes: constraining uncertainties in pyroclastic eruption parameters, Bulletin of Volcanology, 76, 1–16, 2014.

Le Maitre, R., Bateman, P., Dudek, A., Keller, J., LAMEYRE, L., Sabine, P., Schmid, R., Sorensen, H., Streckeisen, A., Wooley, A., et al.: A classification of igneous rocks and glossary of terms. Recommendations of the IUGS Commission on the Systematics of Igneous Rocks, 1989.

Le Pennec, J.-L., Jaya, D., Samaniego, P., Ramón, P., Yánez, S. M., Egred, J., and Van Der Plicht, J.: The AD 1300–1700 eruptive periods at Tungurahua volcano, Ecuador, revealed by historical narratives, stratigraphy and radiocarbon dating, Journal of Volcanology and Geothermal Research, 176, 70–81, 2008.

Maeno, F., Nakada, S., Nagai, M., and Kozono, T.: Ballistic ejecta and eruption condition of the vulcanian explosion of Shinmoedake volcano, Kyushu, Japan on 1 February, 2011, Earth, Planets and Space, 65, 609–621, 2013.

Morrissey, M. and Mastin, L.: Vulcanian eruptions, in: The encyclopedia of volcanoes, edited by Sigurdsson, H., Houghton, B., McNutt, S., Rymer, H., and J, S., pp. 463–475, Elsevier, 2000.

Murcia, H. F., Borrero, C. A., Pardo, N., Alvarado, G. E., Arnosio, M., and Scolamacchia, T.: Depósitos volcaniclásticos: Términos y conceptos para una clasificación en español, Revista Geológica de América Central, 48, 15–39, 2013.

Myers, M. L., Geist, D. J., Rowe, M. C., Harpp, K. S., Wallace, P. J., and Dufek, J.: Replenishment of volatile-rich mafic magma into a degassed chamber drives mixing and eruption of Tungurahua volcano, Bulletin of Volcanology, 76, 1–17, 2014.

Nelson, S. T. and Montana, A.: Sieve-textured plagioclase in volcanic rocks produced by rapid decompression, American Mineralogist, 77, 1242–1249, 1992.

Newhall, C. G. and Self, S.: The volcanic explosivity index (VEI) an estimate of explosive magnitude for historical volcanism, Journal of Geophysical Research: Oceans, 87, 1231–1238, 1982.

Otto, G. H.: A modified logarithmic probability graph for the interpretation of mechanical analyses of sediments, Journal of Sedimentary Research, 9, 1939.

Palma, J.: Wind Reanalysis, https://vhub.org/resources/windre, accessed: 2013, 2013.

Parra, R., Bernard, B., Narváez, D., Le Pennec, J.-L., Hasselle, N., and Folch, A.: Eruption Source Parameters for forecasting ash dispersion and deposition from vulcanian eruptions at Tungurahua volcano: Insights from field data from the July 2013 eruption, Journal of Volcanology and Geothermal Research, 309, 1–13, 2016.

Polacci, M.: Constraining the dynamics of volcanic eruptions by characterization of pumice textures, Annals of Geophysics, 2005.

Pyle, D.: Sizes of volcanic eruptions, Encyclopedia of Volcanoes, 1, 263–269, 2000.

Pyle, D. M.: The thickness, volume and grainsize of tephra fall deposits, Bulletin of Volcanology, 51, 1–15, 1989.

Pyle, D. M.: Assessment of the minimum volume of tephra fall deposits, Journal of Volcanology and Geothermal Research, 69, 379–382, 1995.

Rose, W., Self, S., Murrow, P., Bonadonna, C., Durant, A., and Ernst, G.: Nature and significance of small volume fall deposits at composite volcanoes: Insights from the October 14, 1974 Fuego eruption, Guatemala, Bulletin of Volcanology, 70, 1043–1067, 2008.

Samaniego, P., Le Pennec, J., Barba, D., Hall, M., Robin, C., Mothes, P., Yepes, H., Troncoso, L., and Jaya, D.: Mapa de los peligros potenciales del volcán Tungurahua, Esc, 1, 2008.

Samaniego, P., Le Pennec, J.-L., Robin, C., and Hidalgo, S.: Petrological analysis of the pre-eruptive magmatic process prior to the 2006 explosive eruptions at Tungurahua volcano (Ecuador), Journal of Volcanology and Geothermal Research, 199, 69–84, 2011.

Shand, S. J.: Eruptive Rocks: Their Genesis, Composition, Classification, and Their Relation to Ore-deposits, Thomas Murby, 1949.

Sparks, R. and Walker, G.: The significance of vitric-enriched air-fall ashes associated with crystal-enriched ignimbrites, Journal of Volcanology and Geothermal Research, 2, 329–341, 1977.

Sparks, R. S. J., Bursik, M., Carey, S., Gilbert, J., Glaze, L., Sigurdsson, H., and Woods, A.: Volcanic plumes, Wiley, 1997.

Vallejo, S., Naranjo, F., Ramón, P., Yépez, H., Hidalgo, S., Anzieta, J., Bernard, B., Narváez, D., Mothes, P., and Douillet, G.: The vulcanian eruption of February 1st, 2014 at Tungurahua Volcano, Ecuador, in: Abstract book, Cities on Volcanoes 8, Jogjakarta, Indonesia, 2014.

Walker, G. P.: Grain-size characteristics of pyroclastic deposits, The Journal of Geology, pp. 696–714, 1971.

Wright, H. M., Cashman, K. V., Rosi, M., and Cioni, R.: Breadcrust bombs as indicators of Vulcanian eruption dynamics at Guagua Pichincha volcano, Ecuador, Bulletin of Volcanology, 69, 281–300, 2007.

Zobin, V. M., Carrasco-Núñez, G., and Vargas-Gutiérrez, V. R.: Field and seismic evaluation of the block-and-ash flows emplaced from eruption columns of the 2005 Vulcanian explosions at Volcán de Colima, Mexico, Bulletin of Volcanology, 78, 1–9, 2016.